Localized Measurement of Breathing Movement Using RFID: Proof-of-Concept and Challenges

Citation for the original published paper (version of record):
Zeng, X., Wu, J., Thelandersson, A. et al (2026). Localized Measurement of Breathing Movement Using RFID: Proof-of-Concept and Challenges. IEEE Access, 14: 12655-12663.
http://dx.doi.org/10.1109/ACCESS.2026.3654654

(article starts on next page)

IEEE Access
Multidisciplinary ⋮ Rapid Review ⋮ Open Access Journal

Received 19 November 2025, accepted 7 January 2026, date of publication 15 January 2026, date of current version 27 January 2026.

Digital Object Identifier 10.1109/ACCESS.2026.3654654

RESEARCH ARTICLE

Localized Measurement of Breathing Movement Using RFID: Proof-of-Concept and Challenges

XUEZHI ZENG[1], (Member, IEEE), JIAQI WU[1], ANNELI THELANDERSSON[2], GUNILLA KJELLBY WENDT[1,3], AND MONIKA FAGEVIK OLSÉN[4,5]

[1]Department of Electrical Engineering, Chalmers University of Technology, 412 96 Gothenburg, Sweden
[2]Department of Research, Development, Education and Innovation, Simulation Centre, Sahlgrenska University Hospital, 416 85 Gothenburg, Sweden
[3]Department of Occupational Therapy and Physiotherapy, Sahlgrenska University Hospital, 431 80 Gothenburg, Sweden
[4]Department of Health and Rehabilitation, Institute of Neuroscience and Physiology, University of Gothenburg, 413 46 Gothenburg, Sweden
[5]Department of Occupational Therapy and Physiotherapy, Sahlgrenska University Hospital, 413 45 Gothenburg, Sweden

Corresponding author: Xuezhi Zeng (xuezhi@chalmers.se)

This work was supported in part by the Area of Advance in Health Engineering at Chalmers University of Technology under Grant SOH C 2025-0025-5.

ABSTRACT Measurement of breathing movement is important for the study of breathing mechanics, the diagnosis, and monitoring of respiratory disorders. Conventional imaging-based methods, such as ultrasound and computed tomography, are either bulky and expensive or highly operator- and position-dependent. In this work, we propose a novel and cost-effective method for measuring local breathing movements, leveraging the well-known radio-frequency identification (RFID) technology. We demonstrate the proof-of-concept by using multiple tags to track localized breathing movements in an experimental study with a medical mannequin. The results indicate that RFID technology can enable accurate breathing measurements under some conditions. However, commercial RFID devices are susceptible to multipath interference, which significantly limits measurement stability and robustness. Reliable measurements in practical settings will require custom-developed system solutions.

INDEX TERMS Displacement measurement, respiratory disease, RFID tags, rehabilitation.

I. INTRODUCTION

Many patients suffer from diseases that impact respiratory function. The primary groups affected are individuals with restrictive or obstructive lung diseases. For example, Chronic Obstructive Pulmonary Disease (COPD) is one of the most prevalent lung conditions worldwide and the third leading cause of death globally [1]. Patients with other diagnoses may also have impaired respiration due to musculoskeletal changes in the thorax and spine [2], [3]. In addition, neurological diseases and trauma often lead to respiratory deterioration, and nearly all patients undergoing anesthesia and surgery experience postoperative restrictive lung function [4], [5]. Measurement and monitoring of these patients' respiratory function are important for disease assessment, progression tracking, treatment design, and evaluation of treatment effects.

The associate editor coordinating the review of this manuscript and approving it for publication was Zahra Shaterian.

Various methods are available for measuring changes in lung function. Static and dynamic spirometry are widely used and well-investigated [6]. It gives valuable information about lung volumes and airflow, helping identify pathological conditions. Another way to obtain critical information about respiratory health and lung function is by measuring breathing movements. Unlike airflow measurements (e.g., spirometry), which require active breathing maneuvers, monitoring breathing movements is non-invasive and can be used in various settings.

Various medical devices, including ultrasonography [7], infrared cameras [8], and parallel transaxial CT scans [9], have been utilized to assess chest wall motion during respiration. However, these systems are typically bulky, expensive, and/or highly operator-dependent. Wearable solutions, such as Respiratory Inductance Plethysmography (RIP), Piezoelectric respiration sensors (PZT) [10], [11], and Photoplethysmography (PPG) [12], offers a relatively simple, body-worn means of capturing respiratory activity—RIP and

PZT measure chest and abdominal motion directly, whereas PPG provides an indirect surrogate via respiration-induced modulations of the cardiovascular signal. Nevertheless, these techniques generally lack sufficient spatial resolution to distinguish motion in specific thoracic or abdominal regions. This limitation reduces their ability to provide a comprehensive assessment of regional respiratory mechanics, which is particularly important for personalized treatment and rehabilitation.

Emerging approaches for breathing monitoring, involving the use of accelerometers or Doppler radars, have been reported in recent years. A. Siqueira et al. developed a custom micro-controlled system to collect data from ten accelerometers placed at predefined positions on the thorax and abdomen to identify optimal sensor locations for respiratory-waveform estimation [13]. Although this approach can, in principle, capture local breathing movements, its measurement accuracy is a major concern. In addition, the required cable connections substantially restrict the subject's freedom of movement. Doppler radar, on the other hand, offers the opportunity for contactless measurement, which has gained significant attention for remote breathing and heartbeat monitoring over the past decades [14]. A key limitation of this technology is its inability to separate reflections originating from different body parts, particularly when they fall within the same range bin. It has been demonstrated that it is possible to separate the breathing movement of the thoracic chest wall and the abdomen by placing two radars close to the body and positioning them carefully over the respective regions [15]. However, this approach increases the system complexity, and it is challenging to extend the approach to additional measurement locations.

A cost-effective, portable, and user-friendly device capable of accurately measuring breathing patterns at various parts of the chest and abdomen is highly desirable. Such a device would enable more in-depth respiratory analysis of patients suffering from diseases or injuries affecting their respiratory function, which is essential in settings like rehabilitation clinics and primary care. To the best of our knowledge, no commercially available device currently provides such localized and simultaneous measurements.

We propose an innovative approach based on radio frequency identification (RFID) technology to enable local, multi-site breathing movement measurements. RFID technology is widely utilized in retail, supply chain management, and airports for object tracking and logistics [16]. Beyond these traditional applications, RFID also has great potential for sensing purposes, especially in combination with the use of temperature or pressure sensors [17].

Recent studies have demonstrated the feasibility of RFID for remote breathing monitoring of single [18] or multiple mobile users [19], [20] in home environments, primarily focusing on estimating breathing rate.

In contrast, our work targets a more detailed characterization of respiratory dynamics. Instead of merely estimating breathing rate, we investigate whether RFID can accurately measure chest wall displacement at multiple body locations simultaneously, enabling richer analysis of breathing patterns.

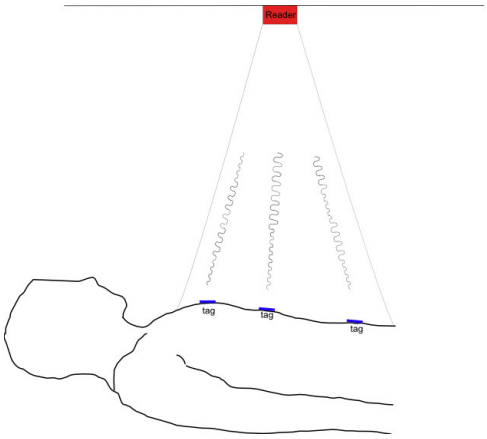

FIGURE 1. Measurement of local breathing movement using multiple RFID tags.

The objective of this work is to demonstrate a proof-of-concept of using RFID technology for localized chest-wall displacement measurement and to quantify its accuracy under controlled conditions using commercial RFID devices and a programmable breathing mannequin. Specifically, we (i) describe the system architecture and signal-processing chain, (ii) evaluate displacement and respiratory pattern estimation at multiple chest locations, and (iii) identify key technical challenges for translation toward clinical use. The remainder of this paper is organized as follows. Section II outlines the fundamental principles of RFID-based motion sensing. Section III describes the experimental study, including the measurement system, setup, signal processing, and accuracy metrics. Section IV presents qualitative and quantitative results. Section V discusses the findings, practical challenges encountered, limitations of the study, and directions for future work. Finally, Section VI concludes the paper.

II. RFID-BASED MOTION SENSING

A typical RFID system consists of a reader (including a reader antenna) and one or more tags, with each tag comprising a chip and an antenna. During operation, the reader emits a radio-frequency signal to activate nearby tags and collects the back-scattered signal [21].

The measurement scenario using multiple tags placed on the body for localized breathing movement measurement is illustrated in Fig. 1.

The transmitted signal can be simply represented by a single frequency wave:

$$T(t) = Asin(\omega t + \alpha) \tag{1}$$

where A represents the amplitude, ω is the angular frequency, and α is the initial phase.

The signal back-scattered by a tag is a modulated and delayed copy of the transmitted signal, but with

a significantly reduced amplitude governed by the following radar equation [22]:

$$P_r = \frac{P_t G^2 \lambda^2 \sigma}{(4\pi)^3 R^4} \tag{2}$$

where P_t is the transmitted power, G is the gain of the reader antenna, λ is the wavelength, σ is the radar cross-section (RCS) of the tag, and R is the distance of the tag to the reader.

Once the tag is activated by harvesting sufficient power from the reader, it modulates its radar cross-section according to the encoded data—a sequence of binary ''0''s and ''1''s. Consequently, the backscattered signal alternates between a high-RCS state (representing, for example, ''1'') and a low-RCS state (representing ''0''), allowing the reader to decode the transmitted data. The backscattered signal from the tag can be expressed as follows:

$$R(t) = B(t)sin[\omega(t - \Delta) + \alpha] \tag{3}$$

Here $B(t)$ represents the amplitude of the back-scattered signal. $\Delta = \frac{2R}{c}$ is the time delay between the back-scattered signal and the transmitted signal, given that c represents the speed of light.

When a person breathes, the distance between the tag and the reader, R, will change in line with the up and down movement of the chest wall, and this change will result in a phase modulation of the backscattered signal. The relationship between the displacement and the associated phase is:

$$\Delta\Phi(t) = \frac{2\omega\Delta R(t)}{c} \tag{4}$$

Here $\Delta R(t)$ represents the chest wall displacement and $\Delta\Phi(t)$ is the associated phase variation.

Therefore, by demodulating the phase of the received signal, the breathing pattern can be extracted. As each tag has a unique ID (the sequence of binaries), it is possible to identify and distinguish the back-scattered data from multiple tags.

III. EXPERIMENTAL STUDY

To establish the proof-of-concept, an experimental study was conducted in the simulation center of Sahlgrenska University Hospital using commercial RFID devices. A signal processing algorithm was developed to process and analyze the data to generate the quantitative measures and metrics of interest for evaluations.

A. MEASUREMENT SYSTEM AND SETUP

The measurement system is composed of an Impinj Speedway Revolution reader R402 [23], an RFID reader antenna ALR-8698 from Alien technology, and several RFID tags AD Belt M730 from Avery Dennison Smartrac. The reader operates within the UHF frequency band (860–960 MHz) and supports the EPC Gen2v2 protocol (ISO/IEC 18000-63), allowing for fast and reliable reading of multiple tags simultaneously [24]. The antenna's transmit power and receive sensitivity were set to maximum. Dual-target search mode was employed to reduce collisions between tags. The reader operated in its most robust mode, dynamically balancing sensitivity and throughput according to the RF environment. The RFID tags are completely passive; they do not generate or radiate any RF power themselves but simply scatter a portion of the reader's transmitted signal back to the reader antenna.

A medical simulation mannequin was used as the measurement subject. The mannequin is the SimMan 3G from Laerdal Medical [25], and it is an advanced patient simulator designed for simulation training of medical professionals. It can simulate a range of physiological symptoms and can be programmed to breathe at predefined frequencies. It also allows asymmetric breathing to be introduced by deactivating one side of the respiratory system. This setup enables controlled testing of the proposed method under various breathing frequencies and conditions.

Two RFID tag placement scenarios were investigated:

- Two-tag scenario: Two RFID tags were placed symmetrically on the left and right sides of the mannequin's chest wall, approximately a few centimeters below the nipple line.
- Four-tag scenario: Four RFID tags were positioned on the chest wall, with two tags at the left upper (LU) thoracic and right upper (RU) thoracic positions, and two tags at the left lower (LL) thoracic and right lower (RL) thoracic positions.

The tags were placed at predefined positions based on [26], which identified the bilateral third ribs, the xiphoid-process level, and points lateral to the umbilicus as relevant anatomical landmarks on the anterior thoracoabdominal wall. These levels are commonly used in respiration measurements, and bilateral placements at each level are desirable to enable asymmetry detection. Because the medical simulation mannequin does not reproduce abdominal respiratory motion, the present study focused primarily on the thoracic region.

In both scenarios, the RFID reader antenna was mounted on a table approximately 30 cm above the mannequin's chest wall, as illustrated in Fig. 2. To provide a ground truth reference of the breathing patterns, a piezoelectric respiration (PZT) belt manufactured by PLUX Biosignals was attached to the mannequin's chest wall.

B. SIGNAL PROCESSING AND ANALYSIS

The data obtained with the RFID system mainly consists of Received Signal Strength Indicator (RSSI) in dB and phase in radians. The former represents the strength of the signal received by the reader from the tag, and the latter is associated with the propagation delay of the signal.

When a tag moves along with the chest wall or abdomen under breathing, the distance R between the reader and the tag varies over time, resulting in changes in both the RSSI and phase according to (2) and (4). In this work, the phase

FIGURE 2. Experimental setup for the four-tag placement scenario. The breathing pattern is measured by both the RFID system and a PZT belt. The reader antenna, tags, and PZT belt were highlighted with black, red, and yellow dashed outlines, respectively.

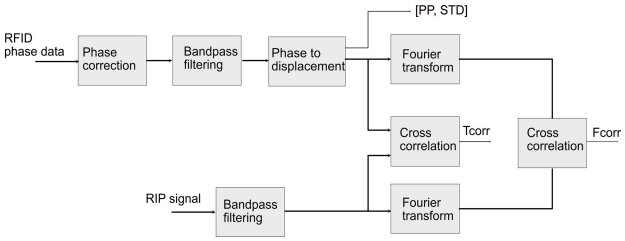

FIGURE 3. Block diagram of the signal-processing and analysis chain.

data is used to extract the breathing information as it is more sensitive to the distance change than the RSSI.

To extract features of interest and evaluate the measurement quality, the acquired data needed to be processed and analyzed. Fig. 3 shows a block diagram of the signal processing algorithm, consisting of:

1) PHASE CORRECTION

The phase data obtained from the RFID reader is not always correct. Instead, it is subject to an inherent ambiguity or offset, where values may be shifted by $\pm 180°$ or $\pm 360°$, resulting in discontinuities. The top panel in Fig. 4 illustrates such an example.

The following algorithm was developed for phase correction to remove the phase offsets caused by the RFID system ambiguity or phase wrapping effect:

- Phase Ambiguity Correction: If the difference between two consecutive phase values lies within the range of 90° to 270°, it is considered a phase ambiguity caused by the reader aliasing effect. Depending on the sign of the difference, a correction of $\pm 180°$ is applied to resolve the ambiguity.
- Phase Unwrapping: If the difference between two consecutive phase values exceeds 270°, a correction of $\pm 360°$ is applied to reconstruct the continuous signal trajectory.

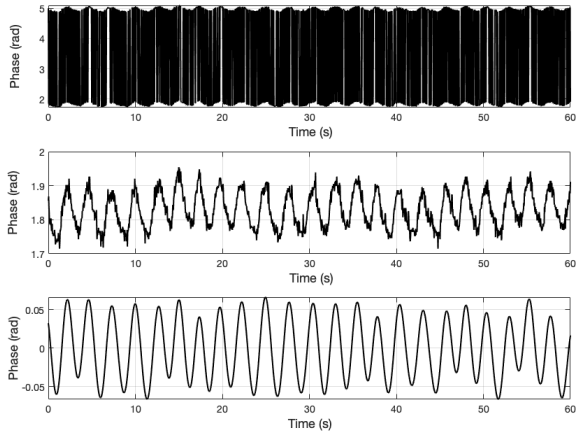

FIGURE 4. Measurement example illustrating the effect of each step of the signal processing algorithm. From top to bottom, the panels show the raw phase data from the RFID system, the phase signal after phase correction, and the filtered phase signal.

The middle panel in Fig. 4 shows the correct phase regained after applying the algorithm.

2) REMOVAL OF DRIFT AND NOISE

The corrected phase data contains low-frequency drift and high-frequency noise. To remove these components, a Butterworth band-pass filter was applied. To preserve the waveform shape, zero-phase filtering was used to eliminate phase distortion (group delay) that occurs in ordinary filtering. The filter bandwidth was set to [3, 30] BPM, covering the breathing rate range used in the experimental study. The bottom panel in Fig. 4 shows the phase signal after filtering. For a fair comparison, the same filter was applied to both the RFID and PZT signals.

3) QUANTITATIVE MEASURES AND METRICS

The filtered phase signal is then converted to displacement according to (4).

To evaluate measurement quality, four quantitative measures (or metrics) were defined: (1) peak-to-peak amplitude (PP), calculated as the difference between the maximum and minimum values of the measured signal; (2) standard deviation (STD); (3) Pearson correlation coefficient between the RFID-derived displacement signal and the PZT signal (T_{corr}); and (4) Pearson correlation coefficient between the frequency spectra of the RFID-derived and PZT signals (F_{corr}). The first two measures characterize changes in chest wall displacement under different conditions, while the latter two metrics assess the similarity between the RFID-based measurements and the reference data.

IV. RESULTS

Qualitative and quantitative results are presented in this section for both the two-tag and four-tag placement scenarios.

A. RESULTS FOR TWO-TAG SCENARIO

Fig. 5 shows a representative measurement example for asymmetry detection. A baseline measurement was first

conducted when both sides of the respiratory system were activated, simulating normal breathing. The measurement was performed twice, and the measurement length was one minute. The same procedure was repeated with the right side of the respiratory system deactivated. The predefined breathing rate is $f_b = 12$ BPM.

Fig. 5a and Fig. 5c are the measured displacement signal from one baseline test in comparison with the PZT signals in the time domain and frequency domain, respectively. Fig. 5b and Fig. 5d present the corresponding results when the right side of the respiratory system was deactivated. In all the sub-figures, the top panel is the PZT signal, the middle and bottom panels are the measurement results for the left side and right side of the chest wall, respectively. To account for measurement instability, the first ten seconds of the recorded signals were discarded.

The results demonstrate that the chest wall displacement measured by RFID closely follows the temporal characteristics of the PZT signal. The frequency spectra in Figs. 5c and 5d further confirm the strong agreement between the RFID-based and PZT-based measurements.

By comparing Fig. 5b to Fig. 5a, we noticed a more significant decrease in the displacement at the right side of the chest compared with the left side.

Fig. 6 presents the results from another similar measurement example but with a higher breathing rate $f_b = 24$ BPM. Again, good agreement is observed in both the time domain and the frequency domain. The deactivation of the right side of the respiratory system clearly results in a smaller displacement on the right side of the chest wall, shown in Fig. 6b.

Table 1 summarizes the quantitative measures and metrics of all the measurements conducted for six different conditions. Two repeated measurements were performed for each condition, yielding a total of twelve tests. The first column lists the measurement condition, specifying whether both sides of the respiratory system were activated or one side was deactivated. For each frequency, results are reported in two rows, corresponding to the left and right sides of the chest wall, respectively.

To provide a more intuitive measure of the displacement change after deactivation of one side of the respiratory system, we calculated both the absolute change (Δ_{pp} and Δ_{std}) and relative change (Δ'_{pp} and Δ'_{std}) in the peak-to-peak amplitude and standard deviation for the left side and right side of the chest wall. These results are presented in Table 2, where the averages of the two repeated measurements under each condition were used. As in Table 1, data for each frequency are organized in two rows, representing the left and right sides of the chest wall.

B. RESULTS FOR FOUR-TAG SCENARIO

Fig. 7 shows the results of one measurement example where four RFID tags were placed at the chest wall, as illustrated in Fig. 2. The predefined breathing rate $f_b = 24$ BPM.

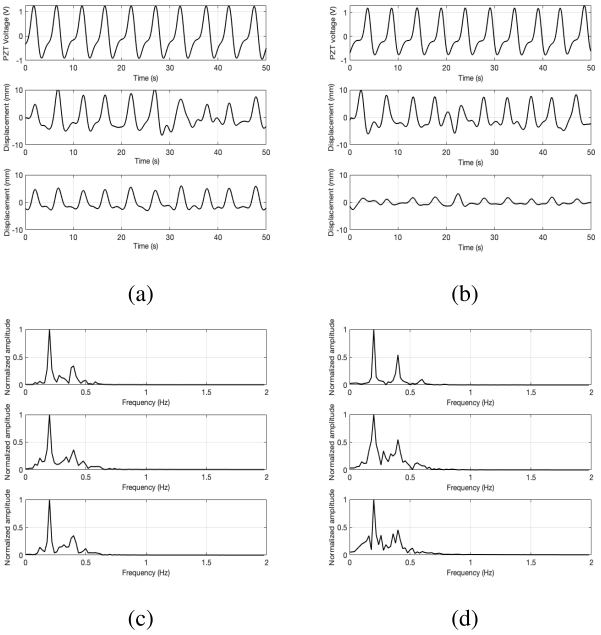

FIGURE 5. Comparison of PZT signals and RFID-based displacement measurements in the time domain and frequency domain for two measurement cases: (a) time domain signals and (c) frequency spectra when both sides of the respiratory system are activated; (b) time domain signals and (d) frequency spectra when the right side of the respiratory system is deactivated. From top to bottom, the panels show the PZT voltage signal (V) and the RFID-based chest-wall displacement on the left and right sides (mm), respectively. The predefined breathing rate is 12 BPM.

Fig. 7a shows the displacement measured by the RFID at the four different locations in comparison with the PZT data when both sides of the respiratory system were activated. Fig. 7b presents the results for a measurement case when the left side of the respiratory system was deactivated. Each figure consists of five panels. From top to bottom, they represent the PZT signal and the displacement signals at the left upper thoracic, right upper thoracic, left lower thoracic, and right lower thoracic positions, respectively.

The results again demonstrate close agreement in temporal patterns between the RFID-based and PZT-based measurements. Distinct reductions in displacement at the left-side positions are clearly visible when the left side of the respiratory system is deactivated.

Table 3 and Table 4 summarize the quantitative measures and displacement changes across all tests, analogous to the results reported in Table 1 and Table 2.

For each frequency, the data are presented in four rows, corresponding to the upper-left (UL), upper-right (UR), lower-left (LL), and lower-right (LR) positions.

V. DISCUSSION

In this section, we discuss the results, highlight the challenges encountered and the limitations of the study, and outline directions for future work.

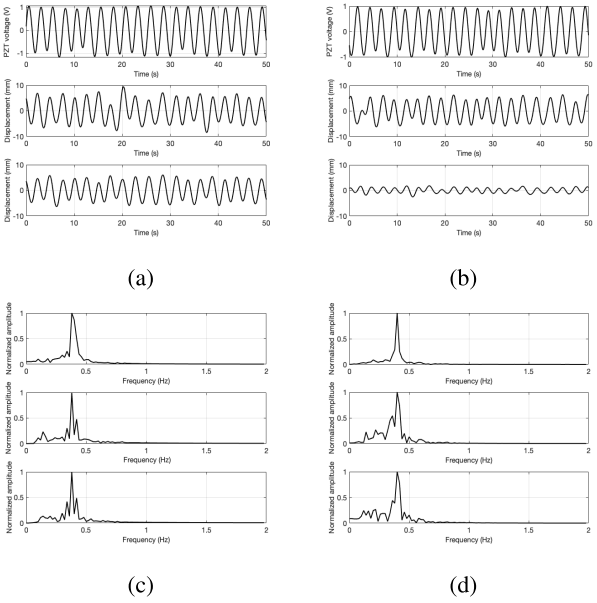

FIGURE 6. Comparison of PZT signals and RFID-based displacement measurements in the time domain and frequency domain for two measurement cases: (a) time domain signals and (c) frequency spectra when both sides of the respiratory system are activated; (b) time domain signals and (d) frequency spectra when the right side of the respiratory system is deactivated. From top to bottom, the panels show the PZT voltage signal (V) and the RFID-based chest-wall displacement on the left and right sides (mm), respectively. The predefined breathing rate is 24 BPM.

A. RESULTS

As shown in Tables 1 and 3, the Pearson correlation coefficients for most measurement cases exceed 0.70, except for a few instances (highlighted in bold), indicating strong similarity between the RFID measurements and the PZT signals in both the time and frequency domains.

The frequency-domain correlation coefficients are generally higher than those in the time domain. In many cases, the frequency correlation exceeds 0.90, demonstrating very strong similarity. These results suggest that RFID-based measurements can provide a reliable estimate of the frequency content of breathing signals. The slightly lower correlations in the time domain may be explained by two factors: (1) time-domain signals are more sensitive to noise and artifacts present during measurement, and (2) the PZT belt and the RFID system capture different aspects of chest wall motion. Specifically, the PZT belt measures deformation across a larger portion of the chest circumference, providing a global estimate of chest wall movement, whereas the RFID system measures local displacement at specific tag locations.

For each condition, two repeated measurements were performed. While the repeated measurements often produced closely matching peak-to-peak amplitudes and standard deviations, in some cases the results differed. The standard deviation was generally more stable than the peak-to-peak amplitude, reflecting the susceptibility of RFID-based measurements to interference, noise and artifacts.

TABLE 1. Quantitative measures and metrics of the RFID-based displacement measurements for the two-tag scenario. "on" and "off" indicate activation and deactivation of one side of the respiratory system. "L" and "R" represent the left side and the right sides of the chest wall, respectively.

Test (L/R)	f_b (BPM)	T_{corr}	F_{corr}	PP (mm)	STD (mm)
T1(on/on)	12	L: 0.87 R: 0.89	L: 0.96 R: 0.98	L: 17.06 R: 9.02	L: 3.92 R: 2.56
T2(on/on)	12	**L: 0.60** R: 0.73	L: 0.77 R: 0.87	L: 8.39 R: 9.09	L: 2.15 R: 2.82
T3(on/off)	12	**L: 0.46** **R: 0.54**	**L: 0.67** R: 0.71	L: 14.26 R: 6.06	L: 2.61 R: 1.14
T4(on/off)	12	L: 0.75 R: 0.73	L: 0.85 R: 0.86	L: 15.91 R: 5.74	L: 3.71 R: 0.96
T5(on/on)	18	L: 0.83 R: 0.84	L: 0.90 R: 0.90	L: 32.03 R: 15.00	L: 9.40 R: 4.49
T6(on/on)	18	L: 0.87 R: 0.88	L: 0.93 R: 0.93	L: 29.12 R: 13.50	L: 9.24 R: 4.34
T7(off/on)	18	L: 0.88 R: 0.89	L: 0.98 R: 0.98	L: 11.52 R: 8.72	L: 3.16 R: 2.24
T8(off/on)	18	L: 0.73 R: 0.71	L: 0.79 R: 0.78	L: 11.15 R: 7.87	L: 3.53 R: 2.28
T9(on/on)	24	L: 0.74 R: 0.75	L: 0.79 R: 0.82	L: 14.78 R: 11.53	L: 4.15 R: 3.13
T10(on/on)	24	L: 0.80 R: 0.81	L: 0.85 R: 0.84	L: 17.90 R: 12.39	L: 4.27 R: 3.49
T11(on/off)	24	**L: 0.41** **R: 0.43**	**L: 0.66** R: 0.70	L: 17.46 R: 5.08	L: 3.88 R: 1.12
T12(on/off)	24	L: 0.75 R: 0.75	L: 0.85 R: 0.87	L: 12.73 R: 4.37	L: 3.72 R: 0.93

TABLE 2. Changes in chest wall displacement on the left side and right sides when one side of the respiratory system is deactivated. A positive value indicates a decrease in the displacement, and a negative value indicates an increase after deactivation. "L" and "R" represent the left side and the right sides of the chest wall, respectively.

f_b (BPM)	Δ_{pp} (mm)	Δ_{std} (mm)	Δ'_{pp}	Δ'_{std}
12	L: -2.36 R: 3.16	L: -0.13 R: 1.64	L: -18.55% R: 34.84%	L: -4.11% R: 60.97%
18	L: 19.24 R: 5.96	L: 5.98 R: 2.16	L: 62.93% R: 41.79%	L: 64.11% R: 48.81%
24	L: 1.25 R: 7.24	L: 0.41 R: 2.29	L: 7.62% R: 60.49%	L: 9.74% R: 69.03%

Despite these disturbances, nearly all measurement cases show substantially larger displacement changes on the side where the respiratory function was deactivated, compared with the opposite side. These consistent results suggest that the RFID system holds strong promise for detecting breathing asymmetry and monitoring changes in breathing patterns.

B. CHALLENGES

We encountered several challenges during the study, including both technical and practical issues.

One of the main challenges was finding an optimal measurement setup. Ideally, the RFID reader should be placed far from the mannequin to maintain an equal distance to all tags. A longer distance is also preferable in practice, as it provides patients and medical staff greater freedom during measurements. However, increasing the reader distance makes the setup more susceptible to multipath interference, which can lead to unstable and noisy measurements. This issue was observed when the reader was mounted on the operating lamp, approximately 90 cm above the mannequin.

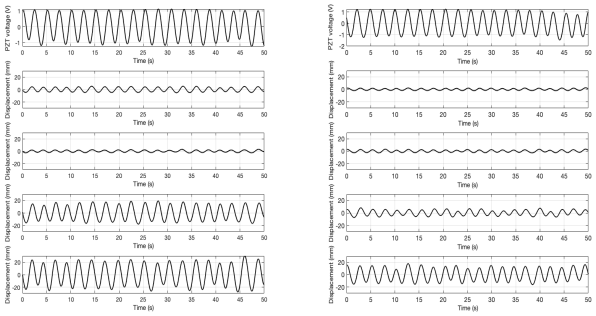

(a) (b)

FIGURE 7. Comparison of PZT signals and RFID-based displacement measurements for two measurement cases in the four-tag scenario: (a) both sides of the respiratory system are activated; (b) the left side of the respiratory system is deactivated. From top to bottom, the panels show the PZT voltage signal (V) and the RFID-based chest-wall displacement at the left upper thoracic, right upper thoracic, left lower thoracic, and right lower thoracic positions (mm), respectively. The predefined breathing rate is 24 BPM.

After testing several configurations, we adopted the setup presented in this work, using a special table with a metal rod as the leg. Although this arrangement improved measurement quality, the proximity of the reader to the metal rod may also have contributed to instability in some cases.

The mannequin's respiratory system was simulated by two balloons. By inflating and deflating the balloons at a controlled rate, we reproduced breathing at a desired frequency, and by deactivating one balloon, we simulated asymmetry. However, because the rubber skin of the mannequin is loosely fitted over the balloons, the movement on one side of the chest wall also affects the other. Consequently, when one side was deactivated, a smaller displacement change was still observed on the opposite side.

Another practical challenge was ensuring good contact between the tags and the mannequin surface. Tags were secured with medical tape, but as they moved with the chest wall, the contact often loosened, resulting in degraded signal quality. Some of the artifacts present in the measurement data may be attributed to this factor. Frequent adjustment or replacement of tape, and occasionally the tags themselves, was required. Notably, a different tag was used in tests T5–T8 (at $f_b = 18$ BPM), where the measurement setup was similar but not identical to that used in the other tests summarized in Table 1. This may explain why the difference between the displacement changes at the left and right side is smaller at 18 BPM compared with others in Table 2.

C. LIMITATIONS AND FUTURE WORK

The present study has several limitations that need to be addressed before this technology can be deployed in clinical use.

1) TECHNICAL ASPECTS

The results highlight the strong potential of RFID technology for local breathing measurement. However, the prototype used in this study is based on commercial RFID devices designed for entirely different application scenarios, which introduces several limitations that must be addressed in future work.

First, to enhance measurement stability, the reader antenna should have a more directional radiation pattern with low side lobes. A potential solution is to use a lens antenna, which concentrates RF energy into a narrow beam in a specified direction. This would substantially reduce multipath interference and lead to more stable and reliable measurements.

Second, a custom-developed RFID reader is desirable, as it would provide flexibility in adjusting system parameters

TABLE 3. Quantitative measures and metrics of the RFID-based displacement measurements for the four-tag scenario. "on" and "off" indicate activation and deactivation of one side of the respiratory system. "LU", "RU", "LL", and "RL" represent the left upper thoracic, right upper thoracic, left lower thoracic, and right lower thoracic positions, respectively.

Test (L/R)	f_b(BPM)	T_{corr}	F_{corr}	PP(mm)	STD(mm)
F1(on/on)	12	LU:0.73 RU:0.76 LL:0.77 RL:0.75	LU:0.93 RU:0.94 LL:0.93 RL:0.93	LU:8.29 RU:5.58 LL:29.99 RL:71.08	LU:2.62 RU:1.62 LL:9.10 RL:20.83
F2(on/on)	12	LU:0.85 RU:0.85 LL:0.82 RL:0.84	LU:0.96 RU:0.96 LL:0.95 RL:0.96	LU:8.64 RU:4.70 LL:27.95 RL:65.58	LU:2.55 RU:1.38 LL:8.25 RL:18.22
F3(off/on)	12	LU:0.80 RU:0.83 LL:0.80 RL:0.82	LU:0.96 RU:0.98 LL:0.96 RL:0.97	LU:4.41 RU:6.64 LL:14.27 RL:32.23	LU:1.14 RU:1.77 LL:3.80 RL:8.84
F4(off/on)	12	LU:0.80 RU:0.80 LL:0.83 RL:0.79	LU:0.97 RU:0.97 LL:0.97 RL:0.96	LU:4.13 RU:6.53 LL:13.82 RL:34.35	LU:1.15 RU:1.72 LL:3.75 RL:9.42
F5(on/on)	24	LU:0.70 RU:0.72 LL:0.78 RL:0.72	LU:0.83 RU:0.80 LL:0.83 RL:0.82	LU:10.58 RU:5.98 LL:37.28 RL:58.04	LU:3.12 RU:1.53 LL:11.01 RL:16.13
F6(on/on)	24	**LU:0.22** **RU:0.20** **LL:0.21** **RL:0.20**	**LU:0.46** **RU:0.40** **LL:0.39** **RL:0.42**	LU:11.01 RU:5.87 LL:44.43 RL:61.31	LU:3.00 RU:1.43 LL:11.56 RL:15.62
F7(off/on)	24	LU:0.71 RU:0.70 LL:0.70 **RL:0.64**	LU:0.79 RU:0.76 LL:0.79 RL:0.70	LU:4.58 RU:6.01 LL:15.66 RL:34.95	LU:1.30 RU:1.75 LL:3.77 RL:9.31
F8(off/on)	24	**LU:0.57** **RU:0.58** **LL:0.60** **RL:0.60**	LU:0.90 RU:0.89 LL:0.89 RL:0.92	LU:4.69 RU:6.16 LL:15.51 RL:34.16	LU:1.32 RU:1.68 LL:3.97 RL:9.69

TABLE 4. Changes in chest-wall displacement on the left and right sides when one side of the respiratory system is deactivated. A positive value indicates a decrease in the displacement, and a negative value indicates an increase after deactivation. "LU", "RU", "LL", and "RL" represent the left upper thoracic, right upper thoracic, left lower thoracic, and right lower thoracic positions, respectively.

f_b(BPM)	Δ_{pp}(mm)	Δ_{std}(mm)	Δ'_{pp}	Δ'_{std}
12	LU: 4.20 RU: -1.45 LL: 14.93 RL: 35.04	LU: 1.44 RU: -0.25 LL: 4.90 RL: 10.40	LU: 49.56% RU: -28.11% LL: 51.52% RL: 51.28%	LU: 55.71% RU: -16.33% LL: 56.48% RL: 53.24%
24	LU: 6.16 RU: -0.16 LL: 25.27 RL: 25.12	LU: 1.75 RU: -0.24 LL: 7.42 RL: 6.38	LU: 57.06% RU: -2.70% LL: 61.85% RL: 42.09%	LU: 57.19% RU: -15.88% LL: 65.71% RL: 40.16%

for this dedicated application. More importantly, it would enable access to raw data, which is essential for effective noise and artifact suppression through advanced signal processing. A custom reader would also allow exploration of different operating frequencies to identify the optimal range.

Third, commercial RFID tags typically perform poorly when placed directly on the human body due to detuning effects. To enable their use for breathing monitoring, robust methods to mitigate the influence of the skin on tag performance—or redesigned tags—are required to ensure reliable operation.

In addition to these aspects, the availability of ground-truth data is essential for a comprehensive evaluation of the measurement accuracy. Neither the PZT belt nor the simulator provides absolute displacement amplitudes, making it difficult to quantify measurement accuracy. Despite certain limitations, the Respiratory Movement Measuring Instrument (RMMI), based on laser technology [26], can provide reliable measurements at six anatomical sites and thus offers a trustworthy benchmark for the RFID-based approach.

2) CLINICAL TRANSLATION

Beyond the technical aspects, several practical issues need to be considered for clinical translation.

In this proof-of-concept study, the RFID system was occasionally operated at a relatively high transmit power, with an Equivalent Isotropically Radiated Power (EIRP) of approximately 42.5 dBm at 868 MHz. This reflects a convenient prototype configuration rather than an optimized minimum-power setting. According to the 2020 guidelines of the International Commission on Non-Ionizing Radiation Protection (ICNIRP), the reference level for incident power density for the general public in the 400–2000 MHz band is 4.34 W/m^2, averaged over 30 minutes [27]. Under far-field free-space conditions, continuous transmission at this EIRP reaches this level at approximately 0.57 m from the antenna. In our experiments, however, no human subjects were present, and the reader was active for less than 50 % of any 30-minute interval, substantially reducing the time-averaged RF exposure. For future human and clinical studies, we will reduce the transmit power and increase the subject–antenna separation to ensure that participant exposure remains comfortably below the relevant ICNIRP limits under conservative assumptions.

In clinical environments, the RF fields radiated from the reader may interact with other medical devices worn by patients (e.g., implanted cardiac devices, insulin pumps). A dedicated electromagnetic compatibility (EMC) assessment in accordance with relevant standards for active medical devices will therefore be required before clinical deployment. Potential interactions with co-located medical devices thus constitute an important limitation of the present work and a key target for future investigation.

Finally, in the mannequin-based setup used in this study, only breathing-like chest-wall motion was simulated. Gross body movements, posture changes, and soft-tissue deformations beyond the programmed breathing pattern were not modeled. In real-world scenarios—particularly for continuous monitoring—such factors may affect tag coupling and phase stability, potentially degrading measurement accuracy. Evaluating robustness to realistic patient motion and posture variation, and developing methods to mitigate these effects, represent important directions for future work.

VI. CONCLUSION

We assessed the feasibility of using an RFID sensor for measuring local breathing movements.

Our results indicate that the temporal characteristics and frequency spectrum of the RFID-based measurements closely resemble those of the reference signals in most of the measurement cases. Furthermore, we demonstrated that RFID can detect asymmetries in breathing movements and monitor local displacement changes over time.

However, the limitations of commercial RFID devices pose significant challenges for stable and robust measurements in realistic scenarios. If these challenges are properly addressed, this technology can have great value in the diagnostics, monitoring, and treatment of respiratory diseases.

ACKNOWLEDGMENT

The authors would like to thank Axel Klang, Ali Hassani, Hafizullah Alizada, and Usama Khaswan for data collection.

REFERENCES

[1] (2024). *Chronic Obstructive Pulmonary Disease (COPD)*. [Online]. Available: https://knowledge-action-portal.com/en/content/chronic-obstructive-pulmonary-disease-copd

[2] L. S. Avnon, F. Manzur, A. Bolotin, D. Heimer, D. Flusser, D. Buskila, S. Sukenik, and M. Abu-Shakra, "Pulmonary function testing in patients with rheumatoid arthritis," *ISR Med. Assoc. J.*, vol. 11, pp. 83–87, Jan. 2009.

[3] S. Takahashi, N. Suzuki, T. Asazuma, K. Kono, T. Ono, and Y. Toyama, "Factors of thoracic cage deformity that affect pulmonary function in adolescent idiopathic thoracic scoliosis," *Spine*, vol. 32, no. 1, pp. 106–112, Jan. 2007.

[4] M. Fagevik Olsén, "Chest physical therapy in surgery: A theoretical model about who to treat," *Breathe*, vol. 1, no. 4, pp. 308–314, Jun. 2005.

[5] K. L. Stolzmann, D. R. Gagnon, R. Brown, C. G. Tun, and E. Garshick, "Longitudinal change in FEV1 and FVC in chronic spinal cord injury," *Amer. J. Respir. Crit. Care Med.*, vol. 177, pp. 781–786, Jan. 2008.

[6] P. H. Quanjer, G. J. Tammeling, J. E. Cotes, O. F. Pedersen, R. Peslin, and J.-C. Yernault, "Lung volumes and forced ventilatory flows," *Eur. Respiratory J.*, vol. 6, no. Suppl 16, pp. 5–40, Mar. 1993.

[7] T. Kotani, S. Minami, K. Takahashi, K. Isobe, Y. Nakata, M. Takaso, M. Inoue, S. Nishikawa, T. Maruta, T. Tamaki, and H. Moriya, "Three-dimensional analysis of chest wall motion during breathing in healthy individuals and patients with scoliosis using an ultrasonography-based system," *Stud. Health Technol. Inf.*, vol. 91, p. 135, Jan. 2009.

[8] J. C. Y. Leong, W. W. Lu, K. D. K. Luk, and E. M. Karlberg, "Kinematics of the chest cage and spine during breathing in healthy individuals and in patients with adolescent scoliosis," *Spine*, vol. 24, pp. 1310–1315, Jan. 1999.

[9] T. Kondo, H. Arita, Y. Ohta, and H. Yamabayashi, "Role of the mediastinum as a part of the chest wall: Analyzed by computed tomography," *Respiration*, vol. 56, nos. 1–2, pp. 116–126, 1989.

[10] C. D. Hanning, H. C. Smith, and I. M. Ledingham, "Clinical application of inductive plethysmography," *Scottish Med. J.*, vol. 23, no. 4, pp. 310–311, Oct. 1978.

[11] D. Vitazkova, E. Foltan, H. Kosnacova, M. Micjan, M. Donoval, A. Kuzma, M. Kopani, and E. Vavrinsky, "Advances in respiratory monitoring: A comprehensive review of wearable and remote technologies," *Biosensors*, vol. 14, no. 2, p. 90, Feb. 2024, doi: 10.3390/bios14020090.
[12] SmartQare. *ViQtor (PPG-based)—Monitoring Key Vital Signs*. Accessed: Dec. 10, 2025. [Online]. Available: https://www.smartqare.com/products-and-solutions/meet-viqtor/monitoring-key-vital-signs/
[13] A. Siqueira, A. F. Spirandeli, R. Moraes, and V. Zarzoso, "Respiratory waveform estimation from multiple accelerometers: An optimal sensor number and placement analysis," *IEEE J. Biomed. Health Informat.*, vol. 23, no. 4, pp. 1507–1515, Jul. 2019.
[14] M. Liebetruth, K. Kehe, D. Steinritz, and S. Sammito, "Systematic literature review regarding heart rate and respiratory rate measurement by means of radar technology," *Sensors*, vol. 24, no. 3, p. 1003, Feb. 2024.
[15] Y. S. Lee, P. N. Pathirana, and C. L. Steinfort, "Detection of respiratory paradoxical movement via Doppler radar measurements," in *Proc. 7th Int. Conf. Inf. Autom. Sustainability*, Dec. 2014, pp. 1–5.
[16] R. Want, "An introduction to RFID technology," *IEEE Pervasive Comput.*, vol. 5, no. 1, pp. 25–33, Jan. 2006, doi: 10.1109/MPRV.2006.2.
[17] F. Costa, S. Genovesi, M. Borgese, A. Michel, F. A. Dicandia, and G. Manara, "A review of RFID sensors, the new frontier of Internet of Things," *Sensors*, vol. 21, no. 9, p. 3138, Apr. 2021, doi: 10.3390/s21093138.
[18] S. Zhang, X. Liu, Y. Liu, B. Ding, S. Guo, and J. Wang, "Accurate respiration monitoring for mobile users with commercial RFID devices," *IEEE J. Sel. Areas Commun.*, vol. 39, no. 2, pp. 513–525, Feb. 2021, doi: 10.1109/JSAC.2020.3020604.
[19] C. Zang, C. Zhang, M. Zhang, and Q. Niu, "An RFID-based method for multi-person respiratory monitoring," *Sensors*, vol. 22, no. 16, p. 6166, Aug. 2022, doi: 10.3390/s22166166.
[20] Y. Wang and Y. Zheng, "TagBreathe: Monitor breathing with commodity RFID systems," *IEEE Trans. Mobile Comput.*, vol. 19, no. 4, pp. 969–981, Apr. 2020.
[21] K. Finkenzeller and D. Mulle, *RFID Handbook: Fundamentals and Applications in Contactless Smart Cards, Radio Frequency Identification and Near-Field Communication*. Hoboken, NJ, USA: Wiley.
[22] M. I. Skolnik, *Radar Handbook*, 3rd ed., New York, NY, USA: McGraw-Hill, 2008.
[23] *Impinj Speedway Revolution Reader R402*. Accessed: Dec. 10, 2025. [Online]. Available: https://www.impinj.com/products/readers/impinj-speedway
[24] *EPC UHF Gen2 Air Interface Protocol*. Accessed: Dec. 10, 2025. [Online]. Available: https://www.gs1.org/standards/rfid/uhf-air-interface-protocol
[25] *SimMan 3G*. Accessed: Dec. 10, 2025. [Online]. Available: https://laerdal.com/gb/products/simulation-training/emergency-care-trauma/simman-3g/
[26] M. F. Olsén and K. Romberg, "Reliability of the respiratory movement measuring instrument, RMMI," *Clin. Physiol. Funct. Imag.*, vol. 30, no. 5, pp. 349–353, Sep. 2010.
[27] International Commission on Non-Ionizing Radiation Protection (ICNIRP), "Guidelines for limiting exposure to electromagnetic fields (100 kHz to 300 GHz)," *Health Phys.*, vol. 118, no. 5, pp. 483–524, May 2020, doi: 10.1097/HP.0000000000001210.

XUEZHI ZENG (Member, IEEE) received the Ph.D. degree in electrical engineering from the Chalmers University of Technology, Gothenburg, Sweden, in 2013. She is an Associate Professor (Docent) with the Department of Electrical Engineering, Chalmers University of Technology. Her research interests lie in intelligent RF and multimodal sensing systems for healthcare, with a particular focus on biomedical radar and RF-based physiological sensing combined with AI-driven signal processing and data analytics. Her work targets continuous, contactless health monitoring, including applications in fall-risk assessment, respiratory disease risk prognostics and stratification, and home-based monitoring and rehabilitation. She is an Associate Editor of the IEEE JOURNAL OF ELECTROMAGNETICS, RF AND MICROWAVES IN MEDICINE AND BIOLOGY.

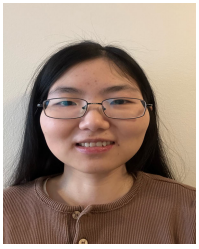

JIAQI WU received the B.Sc. degree in biomedical engineering from Beihang University, China, and the M.Sc. degree in biomedical engineering from the Chalmers University of Technology, Sweden. Her research interests include bioelectronic and sensing technologies for human health monitoring, including non-invasive respiratory signal detection.

ANNELI THELANDERSSON received the Ph.D. degree in medicine in Sweden, in 2016. Her research has mainly focused on physiotherapy at the Intensive Care Unit. She is currently with the Simulation Centre, Department of Research, Development, Education and Innovation, Sahlgrenska University Hospital, Gothenburg, Sweden. She is also a Registered Physiotherapist.

GUNILLA KJELLBY WENDT received the Ph.D. degree. She is currently the Head of the Department of Occupational Therapy and Physiotherapy, Sahlgrenska University Hospital, Sweden, and an Adjunct Professor of adaptive physiotherapy with the Chalmers University of Technology, Sweden. She is also an RPT. Her research interests include rehabilitation outcomes, physiotherapy interventions, and the integration of digital innovations in clinical care.

MONIKA FAGEVIK OLSÉN is currently a Professor with the University of Gothenburg and a Senior Consultant Physiotherapist with Sahlgrenska University Hospital, Sweden. Her research interests include physiotherapy and abdominal surgery.